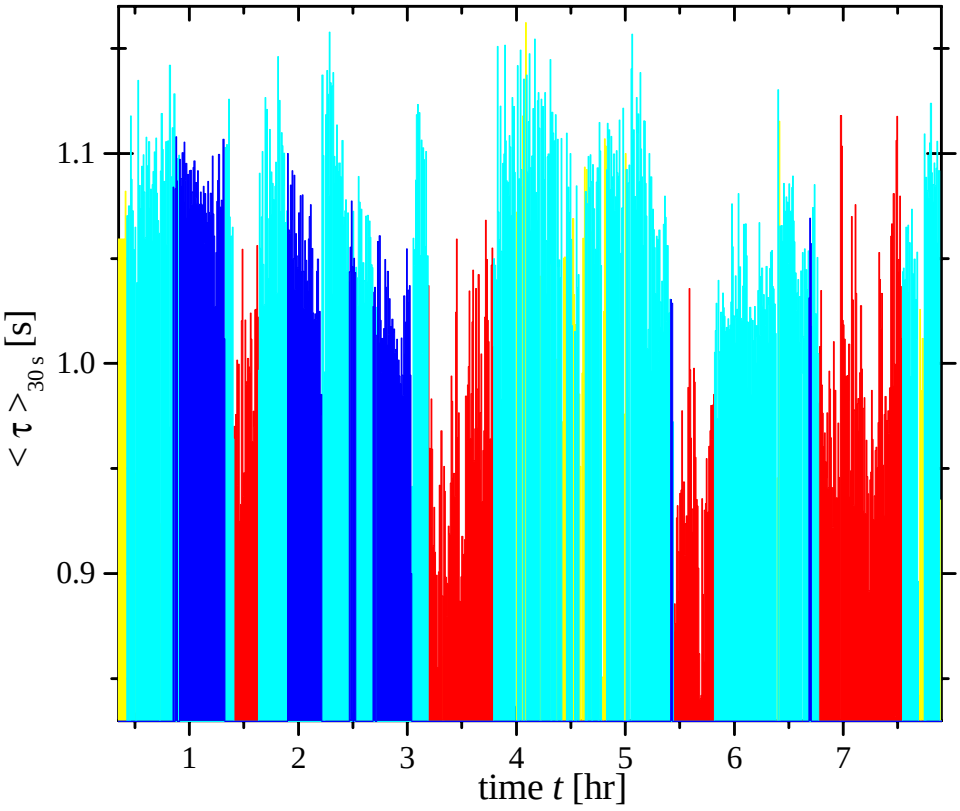
1.1
1.0
0.9
< τ >30 s [s]
1
2
3
4
5
6
7
time t [hr]

8. Physiological Relevance of Scaling of Heart Phenomena

Larry S. Liebovitch, Thomas Penzel, and Jan W. Kantelhardt

Most methods used to analyze experimental data are based on the assumption that the data is from a Gaussian distribution and uncorrelated. We describe methods to analyze data from scaling phenomena that do not have a Gaussian distribution [8.1–8.3] or involve long-range correlations [8.4–8.6]. We then show how those scaling methods have proved useful in characterizing the heart rate data from people who are healthy, from people who have a specific sleep disorder, and from people who have irregular heart rhythms.

8.1 Introduction

We are used to thinking that a single number is the best way to characterize our experimental data. For example, we typically determine the average value of a set of experimental measurements. This basically assumes that most of the values of the data have about this value, with perhaps some a bit larger and others a bit smaller. More specifically, we assume that the data has a Gaussian distribution. When this is the case, as we collect more data, the means of those samples of data approach a finite limiting value that we identify as the characteristic mean of the population, called the population mean. Our best estimate of the population mean is then how we characterize the data.

However, many systems have the universal feature that they extend over many scales. Thus, there is no single value, such as an average value, that can adequately characterize such systems. Such systems are fractal. For example, a tree has an ever larger number of ever smaller branches. There is no single, average value that properly characterizes the diameter of the branches of the

◀ **Fig. 8.0.** A one-night record of heartbeat intervals from a healthy subject with color-coded sleep stages: REM sleep (red), light sleep (light blue), deep sleep (dark blue), and intermediate wake stages (yellow)

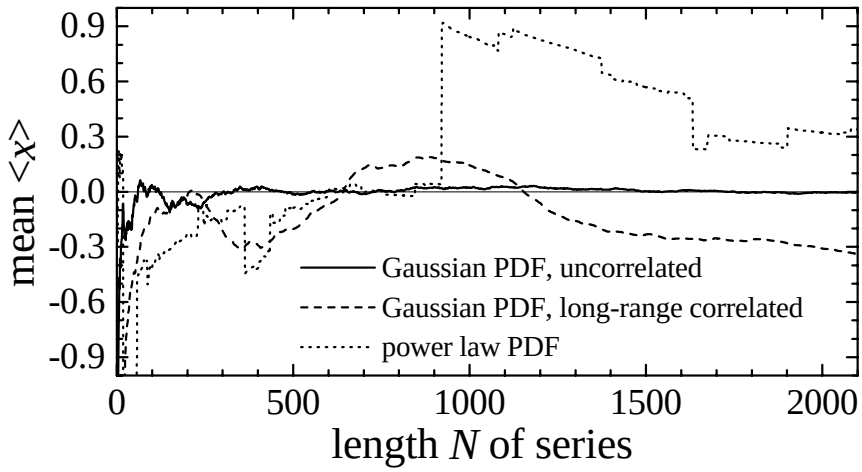

Fig. 8.1. The means $\langle x \rangle$ for three series of random numbers $(x_i), i = 1, \ldots, N$ are shown vs. the length N of the series. While the mean quickly converges to zero for the uncorrelated random data from a Gaussian probability density function (PDF), the means do not converge in the case of random numbers with a power-law PDF or long-range correlated Gaussian distributed numbers. In these cases the data is not described by a mean value but by the Hurst exponent $H = 1.1$, which corresponds to $\beta \approx 1.9$ in the case of the power-law PDF. All PDFs are symmetrical to $x = 0$

tree. A fractal object in space or a fractal process in time has a distribution of values that consist of a few large values, many medium values, and a huge number of small values. More specifically, the data has a distribution that is a power-law, that is, the plot of the logarithm of the relative frequency vs. the logarithm of the values is a straight line. When this is the case, as we collect more data, the means of those samples of data, continue to increase or decrease. The same happens when the data is not power-law distributed but involves long-range correlations, for example, when the probability density for the value at a given time depends on the previous values. The sample means do not approach a finite, limiting value that we can identify as the population mean. This behavior is illustrated in Fig. 8.1. It makes sense because there is no single value that characterizes the many scales spanned by the values of the data. For this case, the meaningful way to characterize the data is to determine how the sample means measured from the data depend on the resolution of the measurement. This can be done by plotting the logarithm of the average fluctuations of the sample means vs. the logarithm of the resolution at which they are determined. If the data is a simple fractal then this plot will be a straight line. If the data is multifractal, that is, consists of many different fractal dimensions, the slope of the straight lines will depend on the moment considered [8.9]. The fractal dimension is related to the slope of that line. The relationship between the slope and the fractal dimension depends on the type of measurement and on the definition of the fluctuations of the sample means. In the case of a power-law distribution of the values, the fractal dimension characterizes the relative frequency of the small values compared to the large

values. For such fractal systems, it is the fractal dimension, rather than the mean, that is the meaningful way to characterize the data. In the case of long-range correlations the fractal dimension characterizes the scaling behavior of the mean, for example, as the Hurst exponent characterizes the fractional Brownian motion.

The properties of the higher moments are also different for experimental data that has Gaussian and fractal distributions. Consider the second moment, the variance, which is a measure of the dispersion in the data. For data with a Gaussian distribution, the variance measured from increasingly large samples of data approaches a finite, nonzero, limiting value. For data with a fractal distribution, the variance measured from increasingly large samples of data continues to increase. Again, the same holds if the data is not power-law distributed but involves long-range correlations. For example, in a fractal time series there are increasingly larger fluctuations over longer time scales. Thus, as the variance is measured over longer time windows, these ever larger fluctuations are included, and the variance measured increases. The properties of uncorrelated data from Gaussian distributions can therefore be properly characterized by the limiting values of their moments, particularly, the mean and variance. These are not meaningful measures for data from fractal distributions or for correlated data. However, data from fractal distributions can be properly characterized by determining how those moments depend on the resolution at which they are measured, which determines their fractal dimension.

8.2 Methods of Scaling Analysis

8.2.1 Probability Density Function

The probability density function (PDF) can be used to determine whether the distribution of experimental data is Gaussian or fractal. $\mathrm{PDF}(x)dx$ is the probability that a measurement has a value between x and $x + dx$. The PDF can be determined from a histogram of how often each range of values is found in the data. This method is limited by the fact that if the bins of the histograms are chosen to be small, then there is too little data at large x, and if the bins of the histogram are chosen to be too large, then the resolution is limited at small x. A better method is to determine the PDF by combining histograms of different binsize [8.7]. The PDF of data that is Gaussian has the form $\mathrm{PDF}(x) \propto (1/2\pi s^2)^{\frac{1}{2}} \exp[-(x-m)^2/2s^2]$ where m is the population mean and s is the population standard deviation. The PDF of data that is fractal has the power-law form

$$\mathrm{PDF}(x) \propto x^{-\beta} \tag{8.1}$$

which is a straight line with a slope β on a plot of $\log[\mathrm{PDF}(x)]$ vs. $\log(x)$.

8.2.2 Autocorrelation Function

In addition to the distribution of the values in the time series (x_i), we are interested in the correlation of the deviations of the values x_i and x_{i+T} from their mean $\langle x \rangle$ with different time lags T. Quantitatively, the correlation in the x_i can be determined by the autocorrelation function

$$C(T) = \left\langle \bar{x}_i \cdot \bar{x}_{i+T} \right\rangle = \frac{1}{N-T} \sum_{i=1}^{N-T} \bar{x}_i \cdot \bar{x}_{i+T} \tag{8.2}$$

for a given time series with length N and $\bar{x}_i \equiv x_i - \langle x \rangle$. If the x_i are uncorrelated, $C(T)$ is zero for $T > 0$. For short-range correlations of the x_i, $C(T)$ declines exponentially and for long-range correlations it declines as a power-law

$$C(T) \propto T^{-\gamma} \tag{8.3}$$

with an exponent $0 < \gamma < 1$. A direct calculation of $C(T)$ is not appropriate due to noise superimposed on the collected data x_i and due to underlying trends of unknown origin. For example, $\langle x \rangle$ need not be constant (as discussed above), which makes the definition of $C(T)$ problematic. Thus, we have to determine the correlation exponent γ indirectly using fractal scaling (dispersion) analysis.

8.2.3 Dispersion Analysis

For values from a time series of data, the moments of samples of the data can be determined as more data is included or as the time resolution of the measurement is changed. For uncorrelated data from a Gaussian distribution, the moments such as the mean and variance, approach finite, limiting values that we identify as the mean and variance of the population. For data from a fractal distribution and long-range correlated data, the moments, m, depend on the time window, T, that is used to measure them. Typically, the average fluctuations of the moments display a scaling relationship of a power-law form, AT^H, which is a straight line on a log-log plot. Several methods of scaling analysis are based on the scaling properties of the second moment, the dispersion. The dispersion can be measured by the mean squared deviation, the relative

dispersion (standard deviation divided by the mean), the Fano factor (variance divided by the mean), or the Hurst rescaled range (maximum minus the minimum value of the running sum of the deviations from the mean divided by the standard deviation). In these methods, the parameter H is determined from the slope on a log-log plot of the dispersion measure vs. the time window over which it is measured.

The parameter H characterizes how the fluctuations in the measured values depend on the length of the data window analyzed. This is related to the fractal dimension, D. The relationship between H and D depends on the method used to measure the dispersion. It also characterizes the fractal correlations in the data. For example, for the Hurst rescaled range method, H is determined as the Hurst exponent. When the increments of a time series are uncorrelated and not taken from a power-law distribution, then $H = 0.5$. When the time series has positive correlations at all time scales, that is, when an increase at any time t is more likely to be followed by an increase at some times $t + T$ later, or when the values are power-law distributed, then $H > 0.5$. This is called persistence. When the values in the record are power-law distributed according to (8.1), $D = 2 - H$, and $\beta = 1 + 1/H$, while in the case of long-range correlations according to (8.3), $\gamma = 2 - 2H$. The same relations hold for the detrended fluctuation analysis (DFA). They allow the determination of the scaling exponents β or γ through dispersion analysis. When the time series has negative correlations, that is, when an increase at any time t is more likely to be followed by a decrease at some times $t + T$ later, then $H < 0.5$. This is called antipersistence.

8.2.4 Hurst Rescaled Range (R/S) Analysis

This is the oldest method of scaling analysis. It has been originally introduced by Hurst et al. in 1965 [8.8], see also [8.9]. As a measure of the dispersion it uses the range, R, which is the difference between the maximum and minimum of the deviation from the mean of the running sum of the values of the time series over a given number of values, T. The rescaled range R/S, is the range, R, divided by the standard deviation, S. The dependence of R/S on T is then found and the Hurst parameter H is then determined as the slope of the plot of $\log(R/S)$ vs. $\log(T)$. This is done by partitioning the total record of N values into $[N/T]$ consecutive segments of T values. The mean, $\langle x \rangle_{n,T}$, and standard deviation, $S_{n,T}$, of the values x_i, in the nth segment are determined from

$$\langle x \rangle_{n,T} = \frac{1}{T} \sum_{i=(n-1)T+1}^{nT} x_i \tag{8.4}$$

and

$$S_{n,T} = \left[\frac{1}{T} \sum_{i=(n-1)T+1}^{nT} \left(x_i - \langle x \rangle_{n,T} \right)^2 \right]^{1/2} . \tag{8.5}$$

For i in the range $(n-1)T + 1 \leq i \leq nT$ then

$$Y_{n,T}(i) = \sum_{k=(n-1)T+1}^{i} x_k - \langle x \rangle_{n,T} , \tag{8.6}$$

the range $R_{n,T}$ in the nth segment can be found from

$$R_{n,T} = \max \left[Y_{n,T}(i) \right] - \min \left[Y_{n,T}(i) \right] , \tag{8.7}$$

and the rescaled range $(R/S)_{n,T}$ can be found from

$$(R/S)_{n,T} = R_{n,T}/S_{n,T} . \tag{8.8}$$

The average rescaled range over all the windows is then given by

$$(R/S)_T = \frac{1}{[N/T]} \sum_{n=1}^{[N/T]} (R/S)_{n,T} . \tag{8.9}$$

The average rescaled range $(R/S)_T$ is calculated for all window sizes T, and the scaling law

$$(R/S)_T \propto T^H \quad \Leftrightarrow \quad \log(R/S)_T \propto H \log T \tag{8.10}$$

allows to determine the Hurst exponent H. As explained above, $H > 0.5$ indicates persistence, while $H < 0.5$ indicates antipersistence.

8.2.5 Detrended Fluctuation Analysis (DFA)

Often experimental data is affected by trends, e.g. slow temperature drifts, that modify the investigated system (for other applications see Chaps. 7 and 5). The human heartbeat is also affected by trends, which are caused by external stimuli and lead to drifts in the mean heart rate. Even rather sudden changes can occur, e.g. when the sleep stage changes. The effects of trends have to be well separated from the intrinsic fluctuations of the system. This task in not easy, since as discussed above the average value of the recorded quantity might

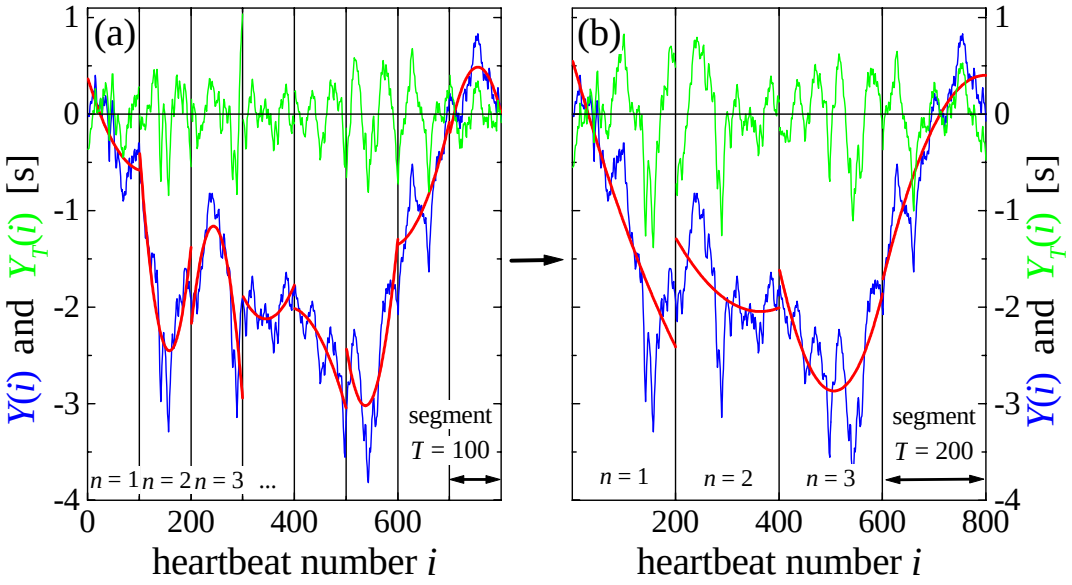

Fig. 8.2. Illustration of the detrending procedure in the detrended fluctuation analysis (DFA). For two segment durations (time scales) $T = 100$ (**a**) and 200 (**b**), the profiles $Y(i)$ (blue lines; defined in (8.11)), least square quadratic fits to the profiles (red lines), and the detrended profiles $Y_T(i)$ (green lines) are shown vs. the heartbeat number i for one record of interbeat intervals for a healthy subject

already be unstable due to the intrinsic fluctuations. Hurst (R/S) analysis works well if we have long records without interruptions or trends. But if trends are present in the data, it might give wrong results. Very often we do not know the reasons for underlying trends in collected data and even worse we do not know the scales of the underlying trends. The underlying trends certainly follow their own laws which can be linear or can have different properties. Detrended fluctuation analysis (DFA) is a well-established method used to determine the scaling behavior for noisy data in the presence of trends without knowing their origin and shape [8.10–8.13].

In the procedure of DFA, we study the profile

$$Y(i) = \sum_{k=1}^{i} x_k - \langle x \rangle \tag{8.11}$$

where $\langle x \rangle$ is the mean of the whole record (x_i) of length T. The second step is performed by cutting the profile $Y(i)$ into $[N/T]$ nonoverlapping segments of equal duration T (see Fig. 8.2). Note that this procedure is rather similar to the (R/S) analysis (cf. (8.6)), except that the splitting of the record is done after the integration. Since the record length N need not be a multiple of the considered time scale T, a short part at the end of the profile will remain. In order not to disregard this part, the same procedure is repeated starting from

the other end of the record, giving $2[N/T]$ segments altogether. In the third step, we calculate the local trend for each segment n by a least-square fit of the data. Then we define the detrended time series for segment duration T, denoted by $Y_T(i)$, as the difference between the original time series and the fits.

Figure 8.2 illustrates this procedure for $T = 100$ and 200. In the example quadratic polynomials are used in the fitting procedure for each segment n, which is characteristic of quadratic DFA (DFA2). Linear, cubic, fourth order, or higher order polynomials can also be used in the fitting procedure (DFA1, DFA3, DFA4, and higher order DFA). Since the detrending of the time series is done by the subtraction of the fits from the profile, these methods differ in their capability to eliminate trends in the data. In qth order DFA, trends of order q in the profile and of order $q-1$ in the original record are eliminated. Thus a comparison of the results for different orders of DFA allows to estimate the strength of the trends in the time series. In the fourth step, we calculate for each of the $2[N/T]$ segments the variance $F_T^2(n) = \langle Y_T^2(i) \rangle$ of the detrended time series $Y_T(i)$ by averaging over all data points i in the nth segment. At last we average over all segments and take the square root to obtain the DFA fluctuation function $F(T)$

$$F(T) = \left[\frac{1}{2[N/T]} \sum_{n=1}^{2[N/T]} F_T^2(n) \right]^{1/2} . \tag{8.12}$$

The fluctuation function is calculated for all possible segment durations $T = 2$ to N. It is apparent, that the variance will increase with increasing duration T of the segments. For long-range power-law correlations in the data $F(T)$ increases by a power-law [8.13]

$$F(T) \propto T^H . \tag{8.13}$$

We can plot $F(T)$ as a function of T with double logarithmic scales to measure H. Hence by measuring the exponent H we can detect the correlation exponent γ from (8.3) or the PDF exponent β from (8.1). For uncorrelated data and short-range correlations, we have $H = 0.5$, while $H > 0.5$ indicates long-range correlations or power-law distributed values. In this way H can be used to investigate correlation properties within a time series.

It is useful to determine if the value of H found from the experimental data is statistically significantly different from that when there are no autocorrelations in the time series. As explained above, a nonsimple scaling behavior (leading to

$H \neq 0.5$ in the dispersion analysis) can be either due to a power-law PDF of the data, to long-range (auto)correlations, or to both. Randomizing the order of the values in the time series (shuffling) will remove the correlations in the data. The time series of the data can be randomized a number of different times and the mean H_m and standard deviation H_s of those time series determined. It is then possible to test the null hypothesis that the H from the time series is the same as the H_m from the uncorrelated surrogate time series. The probability that this is the case is given by probability that $z > |(H - H_m)|/s$ where z is the deviate of the normalized Gaussian distribution. If this probability is large, the nonsimple scaling is not significantly modified by the shuffling. In that case, the deviations from simple scaling with $H = 0.5$ must be due to power-law distributed data. On the contrary, if H is significantly different from $H_m \approx 0.5$, we know that long-range correlations present in the data are responsible for the nonsimple scaling. If H_m is neither close to 0.5 nor to H, both, long-range correlations and a power-law PDF are relevant.

8.3 Heart Rate During Sleep

8.3.1 Heart Rate Regulation

The heartbeat might be thought as a very regular activity solely following the instantaneous needs of the body. However, the measured interbeat intervals do actually fluctuate spontaneously according to the body's needs which themselves are not always very obvious and not completely observable. Not only diseases of the heart itself, but diseases of different origins as well, affect heart rate regulation both in terms of amplitude and variance. The human heartbeat is an essential vital signal which can be assessed over long periods of time using long-term ECG recorders, called a Holter recorder. This type of signal monitoring is now not very expensive and it is now widely available in medicine for clinical investigations and in physiology for research. Thus, this signal can be easily used to investigate the scaling properties and the correlational properties of human biology in healthy subjects and in patient with various diseases.

The heartbeat is regulated by the 'autonomous nervous system'. The autonomous nervous system has two branches, the sympathetic nervous activity which is responsible for heart rate accelerations and the parasympathetic nervous activity which is responsible for heart rate decelerations. These two opposing activities form an autonomic balance which determines the actual heart rate [8.14]. It is thought that these two activities influence the heart rate at different time scales, leading to spontaneous fluctuations of the heart rate.

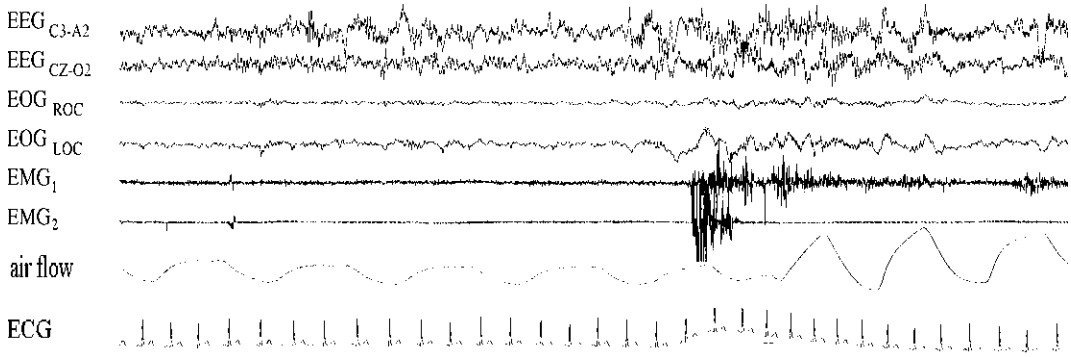

Fig. 8.3. Samples of the recordings taken in the sleep laboratory. The EEG, EOG and EMG records are used to determine the sleep stages, while air flow and ECG records are analyzed

Actually, other influences and reflexes, such as respiration, body temperature regulation, humoral factors and the baroreceptor reflex are also involved in heart rate regulation. When disease is present additional factors can also influence the heart rate regulation. Therefore the model of heart rate regulation driven by sympathetic and parasympathetic activities, as accelerating and decelerating forces, has to be regarded as a simplified concept which helps to understand some, but not all, aspects of heart rate regulation.

The central nervous control of heart rate and blood pressure is located in the cardiovascular center in the brainstem. This center influences sympathetic and parasympathetic activities which control the heart rate and the blood pressure. The respiratory control system, that is also located in the brainstem, controls breathing. The respiratory neurons in the formatio reticularis receive feedback from mechanoreceptors of the lung and the chemoreceptors of the carotid bodies. Both the cardiovascular and the respiratory control centers interact when regulating heart rate, blood pressure and respiration.

Sleep is primarily a condition of rest and has a recreative function for the body and it produces a lower mean value of heart rate. It is assumed that this change is due to the fact that the autonomic balance is shifted towards parasympathetic predominance. Sleep, and its different states of brain activity, affects the cardiovascular and respiratory physiological control systems [8.15].

8.3.2 Sleep Physiology

Sleep is investigated in sleep laboratories where it is possible to continuously record many different physiological measures. These include brain activity (electroencephalogram, EEG), eye movements (electrooculogram, EOG) muscle activity of the chin (electromyogram, EMG submentalis), and the electrical activity of the heart (electrocardiogram, ECG) . In our sleep laboratory we also record respiration with inductive plethysmography, which uses a belt around

the chest to monitor thoracic movements and a belt around the abdomen to monitor abdominal movements. These physiological measures can be used to determine the different sleep states. Figure 8.3 gives an example for some of the recorded signals.

The respiratory movements result in successful inspiration only if the upper airways are maintained open by activating the upper airway muscles located in the throat. The upper airways are collapsible because they also serve the function of swallowing and they play an important role in vocalization. To measure breathing as the result of respiratory movements we record airflow at the nose and the mouth. In addition we record the oxygen content of the blood, called oxygen saturation with a sensor at the finger tip. The muscle activity of legs (EMG tibialis) is recorded to monitor leg movements, which are normal when falling asleep and during changes of body position. A periodic occurrence of leg movements at other times of the night may also disturb sleep. This total set of signals is required for a polysomnography in a sleep laboratory in order to diagnose sleep disorders according to medical recommendations [8.16]. In many sleep laboratories all these parameters mentioned are recorded as a digital time series with digital sampling rates ranging from 1 to 250 samples per second dependent of the signal. The polysomnographic recordings last for 8 to 10 hr and produce large amount of data which must be reviewed by the physician in charge in order to produce a diagnosis and a report.

Based on the recording of EEG, EOG and EMG sleep experts classify sleep states according to rules compiled by committee chaired by Rechtschaffen and Kales in 1968 [8.17]. In order to classify the sleep states the time series are displayed in 30 s segments to the expert. The expert looks at the pattern of the time series visualizing the brain waves, and according to the rules, distinguishes six categories which are awake, sleep stages 1 and 2 (also called light sleep), sleep stages 3 and 4 (also called deep sleep or slow-wave sleep), and REM (rapid eye movement) sleep. In contrast to the other five stages, the sleep expert recognizes REM sleep by reading the rapid eye movements in addition to the brain waves which have a similar pattern to wakefulness. REM sleep is also called paradoxical sleep because the investigated person is still asleep and difficult to arouse even if the brain waves resemble wakefulness. To emphasis the completely different pattern of REM sleep, the other four sleep stages (1 to 4) are summarized as non-REM sleep.

Deep sleep has a physical recreative function. This theory is supported by the finding that all the muscles are relaxed, energy consumption of the body is lowered and many humoral secretions such as growth hormone and stress hormone (cortisol) are activated during non-REM sleep. When awakened during REM sleep, persons report dreaming in 80% of all cases. Even today, there is still controversy as to the function of dreaming and REM sleep. One

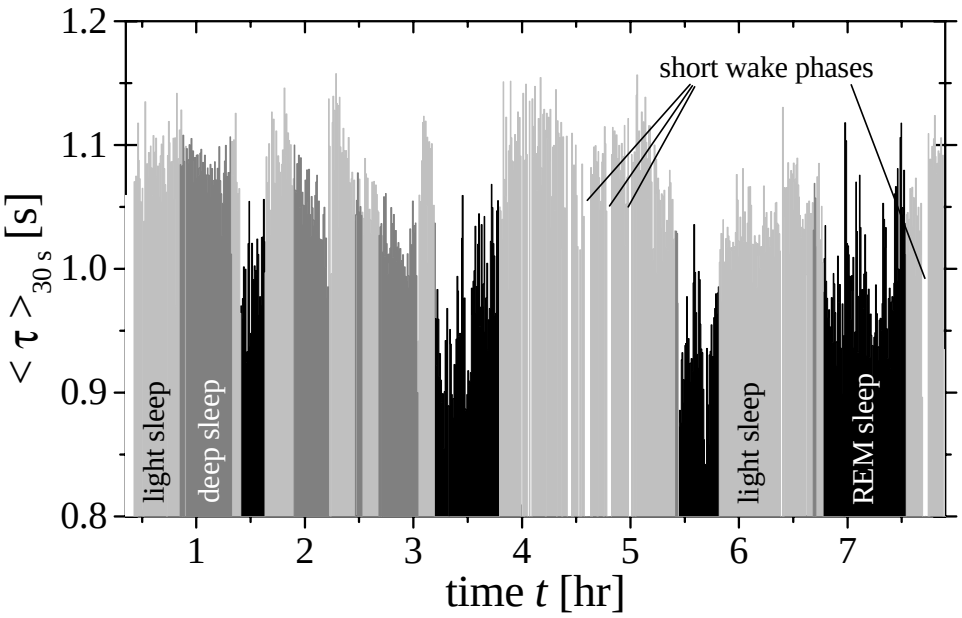

Fig. 8.4. A one-night record of heartbeat intervals from a healthy subject with sleep stages coded underneath the curve. Here RR interval values are averaged over 30 s corresponding to the time resolution of sleep stages. The areas in black mark the REM sleep stages, while light and dark gray have been chosen for light and deep sleep, respectively. It can be observed that the mean of RR intervals is lower in REM sleep than in non-REM sleep, and they fluctuate more strongly

theory says that memory consolidation occurs during REM sleep and thus it has a mental recreative function, while another theory challenges that result [8.18].

In a normal night, sleep stages follow a specific temporal sequence. A few minutes of light sleep follow immediately after falling asleep. These roughly 15 min are only a transition to deep sleep. Deep sleep is maintained for the next 20 to 30 min. Then a few minutes of light sleep are passed as a transition to the first short period of REM sleep which lasts for 5 to 10 min. The entire sequence lasts 90 to 110 min and is called one sleep cycle. Four to six such sleep cycles occur in a normal night of sleep. In the beginning of the night the deep sleep is longer and dominates the sleep cycle. However, in the sleep cycles later in the night REM sleep dominates the cycle and may last 20 to 30 min. No more deep sleep is found in the last third of the night. The duration of light sleep also increases as sleep progresses. Figure 8.4 shows a typical example of the sleep stage pattern for a healthy subject.

8.3.3 Sleep Related Breathing Disorders

One important sleep disorder with a high prevalence of 4% in males and 2% in females within a range of 30 to 60 yr is 'obstructive sleep apnea' [8.19]. This disorder is characterized by cessations of respiratory airflow called apnea, each of which is at least 10 s long [8.16]. These apneas episodes can occur up to 600 times per night [8.16]. During these individual apneas, the respiratory neurons in the brainstem continue to fire and activate the respiratory intercostal muscles and the diaphragm. Therefore, respiratory movements continue during these apneas. But since the upper airways and the pharynx collapse, the respiratory movements are not able to produce a successful ventilation. Because there is no gas exchange in the lung, the oxygen content of the blood decreases during the apnea and this finally causes a central nervous alarm reaction. This causes the brain to wake up and to re-establish respiration. But the patient seldomly becomes aware of these apneas and arousal reactions because the wake up is incomplete and below the level of consciousness.

The changes of respiration during sleep caused by obstructive sleep apnea, influence the autonomous nervous system and the control of heart rate during sleep. This has been established by the direct recording of sympathetic nerve activity with microneurography, a complicated technique which only allows undisturbed recording of nerve activity for a couple of minutes. This method demonstrated the influence of sleep apnea on sympathetic tone. The recordings proved, that during the course of each single apnea, the sympathetic tone increases and after the re-established respiration, the sympathetic tone decreases rapidly [8.20]. The normal reduction of sympathetic tone during sleep is overdriven.

With a much more simple and convenient diagnostic tool, as is the Holter recorder, a typical pattern of heart rate fluctuations was found to be associated with sleep apnea. This pattern is called 'cyclical variation of heart rate' [8.21]. Heart decelerates during the 20 to 60 s of apnea and accelerates during the following 10 to 20 s of breathing following each apnea. This repetitive cyclic pattern is used as an indirect indication for the detection of sleep apnea based on long-term recordings of heart rate, snoring sounds, and oxygen saturation [8.22].

8.3.4 Results for the PDFs

First we present an analysis of the time series of the interbeat intervals τ_i and a calculation of the PDFs of these interbeat intervals in the different sleep stages with their corresponding statistical moments $\langle\tau\rangle$ and $\langle\tau^2\rangle - \langle\tau\rangle^2$. Figure 8.5 shows the PDFs for one healthy subject and one sleep apnea patient. All these distributions have approximately a Gaussian shape. The first and second moments of the PDFs in healthy subjects already allows one to distinguish

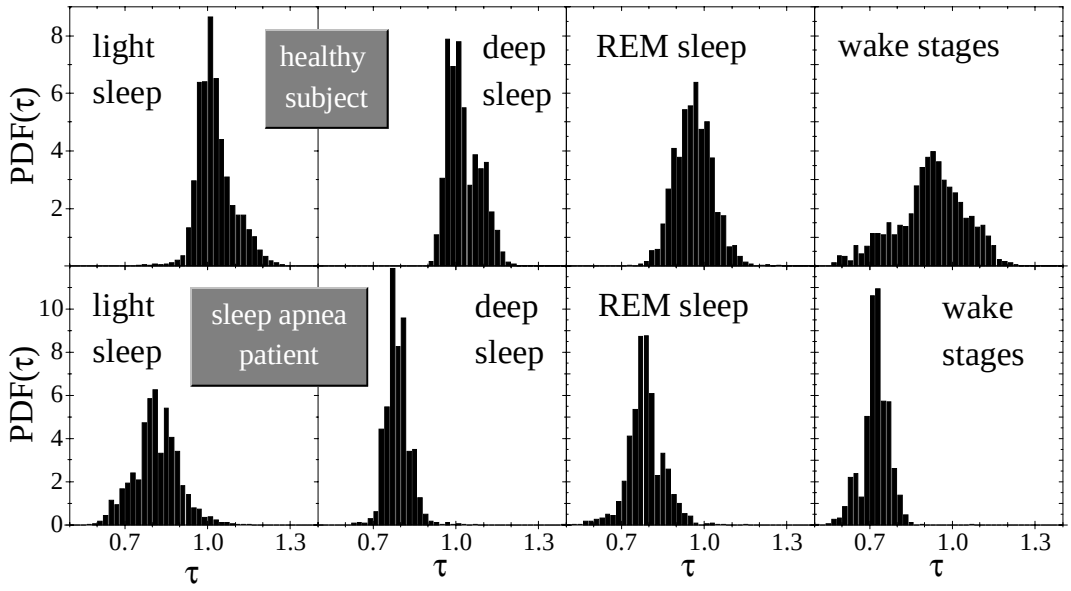

Fig. 8.5. Probability density functions (PDFs) for the heartbeat RR intervals τ_i in the different sleep stages. The first row shows the representative histograms for a one-night recording for a healthy subject, while the second row shows representative data from a sleep apnea patient (with RDI = 33 apneas per hr)

the recordings made during the daytime and during sleep. The mean heart rate is lower and the variance is smaller during non-REM sleep than during wakefulness, as can also be seen in the histograms in Fig. 8.5. Only during REM sleep, does the heart rate increase and the variability is high. In patients with severe obstructive sleep apnea this relation between daytime states and non-REM sleep is reversed. This is caused by the cyclical variation of heart rate associated with the apneas. For the sleep apnea patient in Fig. 8.5 the variability (indicated by the width of the histograms) is largest in light sleep. Unfortunately this effect is not so obvious in patients with moderate or mild sleep apnea and it cannot be found in patients with additional heart diseases that also affect heart rate regulation.

8.3.5 Results from Power Spectrum Analysis and Implications

The power spectrum analysis of heart rate fluctuations provides another way to quantitatively assess the mechanisms of heart rate control [8.23]. Pharmacological blockage of sympathetic and parasympathetic activity and tone is related to specific frequency bands in the power spectrum. Parasympathetic blockage abolishes the mid- (≈ 0.15 Hz) and high frequency (≈ 0.4 Hz) peaks in the power spectrum, whereas sympathetic blockage reduces the low frequency (≈ 0.04 Hz) components of the power spectrum. This finding and other studies have led to recommendations for the interpretation of the spectral analysis of heart rate variability by the European Society of Cardiology and the Ameri-

can Society of Pacing and Electrophysiology [8.24]. The high frequency range is set as 0.15 to 0.4 Hz, the low frequency range is set as 0.04 Hz to 0.15 Hz, the very low frequency range is set as 0.003 to 0.04 Hz and the ultra low frequency range is below 0.003 Hz. It also has been proposed, that these spectral components of heart rate variability provide a measure of the degree of autonomic modulations rather than of the level of autonomic tone.

We also further investigated the textbook description of the progressive decreases of heart rate with sleep stages by using spectral analysis and the frequency bands defined above. It was found that the low frequency components of heart rate variability progressively decrease from wakefulness over sleep stage 1 and sleep stage 2 and reach their lowest values during slow wave sleep. During REM sleep the low frequency components are as high as those during wakefulness. However, the high frequency components of heart rate variability behave just the opposite. They increase from wakefulness over stage 1 and stage 2 to slow-wave sleep. During REM sleep these components are as low as during wakefulness [8.25]. This confirms the theory that high frequency components increase with an increase in parasympathetic activity and low frequency components decrease with a decrease in sympathetic activity. In recent studies heart rate variability was investigated using these frequency bands with the ultimate goal of detecting sleep stage changes based on heart rate changes alone. This ambitious goal has not been reached until now.

Patients suffering from sleep apnea have a specific pattern of heart rate variability associated with their disorder which is called cyclic variation of heart rate [8.21]. Spectral analysis of heart rate variability in patients with sleep apnea was used to identify the periodic changes associated with respiration and with the occurrence of sleep apnea [8.26]. We used nonoverlapping consecutive segments of heart rate recording with a duration of 5 min each. Heart rate was derived from ECG recordings as a part of the polysomnography recordings. The recording of EEG, EOG, EMG, and respiration was used to verify the sleep stages and sleep apnea for each 5 min segment. One peak in the power spectrum, at 0.25 Hz, was identified as the frequency of breathing. A second, more pronounced peak in the power spectrum, was found at 0.015 Hz. This frequency corresponds to the periodicity of apneas which is directly reflected in the cyclical variation of the heart rate. An example for a sleep apnea patient is shown in Fig. 8.6. Thus periods of sleep apnea can be identified using a spectral analysis of heart rate. Having completed this spectral analysis for all segments during the night, then the changes in the frequency of breathing could be observed by the variation of the peak corresponding to the respiratory rhythm. Moreover, the occurrence of sleep apnea could also be followed by the presence or absence of the peak related to the periodicity of sleep apnea. This

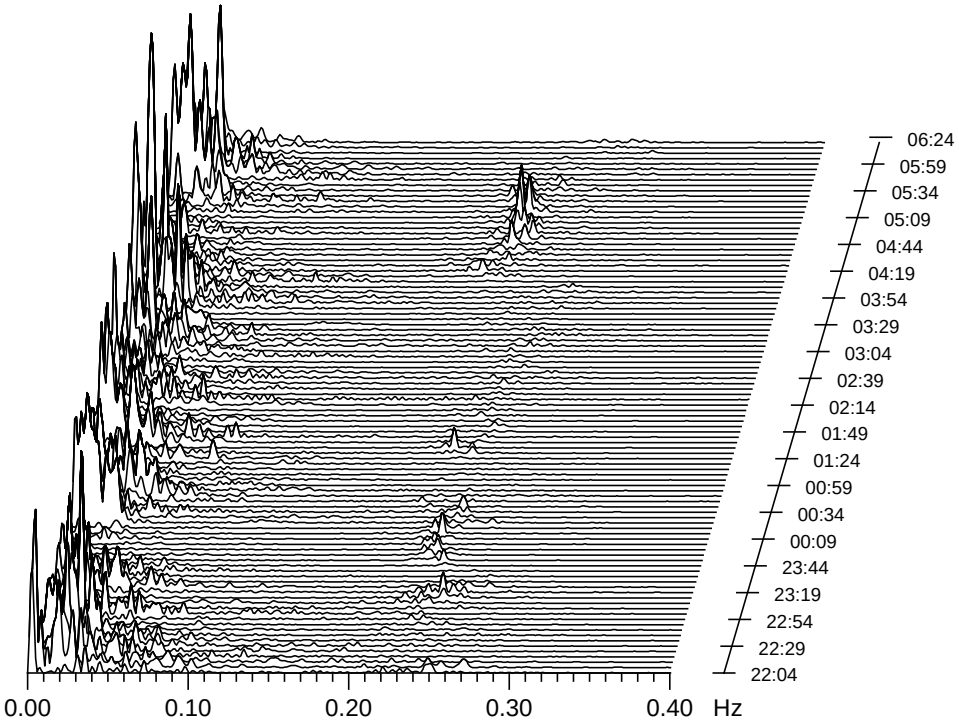

Fig. 8.6. Spectral analysis of heart rate variability in a patient with sleep apnea. The power spectra are shown vs. frequency ν for 20 segments of 5 min duration. The numbers on the right indicate the time of the recordings. The peaks around $\nu \approx 0.25$ Hz show the modulating effect of breathing on the heart rate. The low frequency peaks are caused by apneas. Both effects are modified in intensity and frequency by the sleep stages (not shown)

peak also changed its centre frequency with sleep stages in some patients. We could confirm that the periodicity of apneas did change accordingly in these patients. We can conclude, that spectral analysis of heart rate in patients with sleep apnea allows us to visualize the periodicities in heart rate related to respiration and to sleep apnea. This analysis is less applicable in patients with additional arrhythmic events and with additional heart diseases which cause a reduced heart rate variability.

8.3.6 Results from Dispersion Analysis and Implications

The investigation of the PDFs of the heartbeat intervals (in Fig. 8.5) has shown that they are approximately Gaussian distributed in all sleep and wake stages. Since there are no power-laws involved in the distribution one would not expect any nonsimple scaling behavior. Nevertheless the record of mean interbeat intervals shown in Fig. 8.4 indicates that the mean RR interval is not constant and that the fluctuations might be different in the different sleep stages. In order to investigate the heartbeat fluctuations in the different sleep stages we employed the detrended fluctuation analysis (DFA), since (unknown) trends

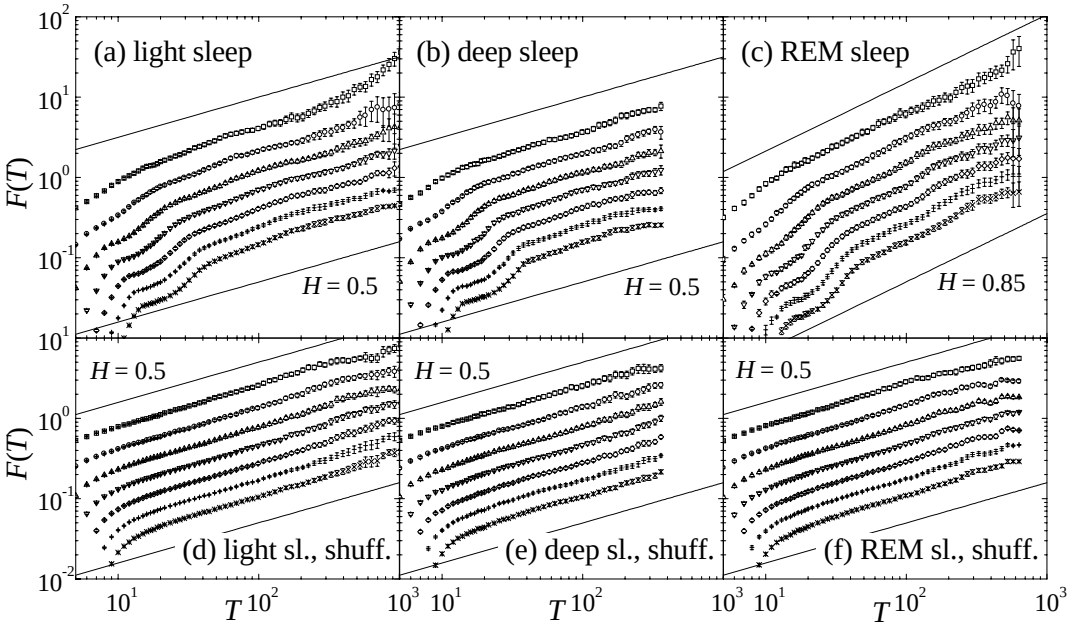

Fig. 8.7. Results of the DFA for a representative healthy subject. The DFA fluctuation functions $F(T)$ for DFA1 (top curves, squares) to DFA7 (bottom curves, crosses) have been plotted vs. the segment duration (time scale) T in log-log plots for (**a**) light sleep, (**b**) deep sleep, and (**c**) REM sleep. Parts (**d**) through (**f**) show the same for surrogate data obtained by shuffling the values of the corresponding records randomly

might be superimposed on the fluctuations (cf. Chaps. 5 and 7). The separation of the sleep stages also eliminated the rather sudden shifts in the heart rate that are due to a change in the sleep stage and not intrinsic to the heartbeat regulation (or the autonomous nervous system) itself.

First we investigated the correlation behavior in the normal volunteers in the different sleep stages [8.6, 8.27]. For many years it had been believed that the fluctuations of the heartbeat intervals are characterized by $1/f$ noise in all sleep and wake stages [8.5, 8.11, 8.28–8.32], and only recently some differences between day and night had been discovered [8.33]. $1/f$ noise corresponds to strong (positive) long-range correlations in the interbeat intervals τ_i. It can equivalently be described by strong long-range anticorrelations in the interbeat interval increments $\delta\tau_i = \tau_i - \tau_{i-1}$. We found that $1/f$ noise is present only for wakefulness and REM sleep which spans 20% of the whole sleep period. In contrast, in non-REM sleep the memory of the heart rates vanishes after a small number of heartbeats corresponding to the typical breathing cycle time, i.e. interbeat intervals separated by more than five heartbeats are actually uncorrelated in deep sleep and light sleep [8.6].

Figure 8.7 shows our results for a representative healthy subject. In light and deep sleep there are only short-range correlations, and we found uncorrelated behavior ($H \approx 0.5$) for larger T, while pronounced long-range correlations

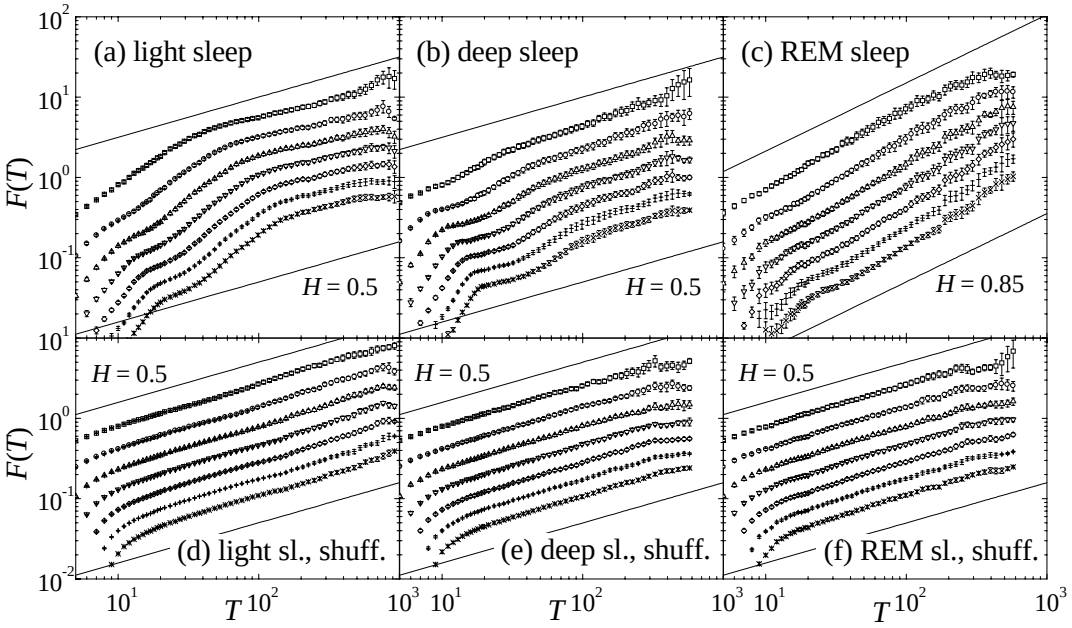

Fig. 8.8. Results of the DFA for a representative sleep apnea patient. For explanation see Fig. 8.7

($H \approx 0.85$) were observed in REM sleep [8.6]. For the higher order DFAs the scaling ranges reach up to the longest accessible time scales, since all trends are removed (see e.g. the $T > 500$ region in (a) for the trend removal). All correlations in the data are perfectly removed by shuffling the data, which indicates that that they are real correlations and not due to some special PDF. The strength of the short-range correlations in light and deep sleep can be estimated by a comparison of the results for the shuffled data.

When we applied detrended fluctuation analysis to patients with sleep apnea, we were surprised to find roughly the same correlation behavior for the sleep stages [8.27], see Fig. 8.8 with the results for a representative sleep apnea patient. Therefore we investigated this in more detail. We compared the correlation behavior in our subjects over two consecutive nights, which is called intraindividual variability and between different healthy subjects, which is called interindividual variability. Still we found the same laws of correlation behavior. The only difference is the range of the short-range correlations, which persist slightly longer for the sleep apnea patients than for healthy subjects (see Figs. 8.7 and 8.8). Also we repeated this comparison for patients with obstructive sleep apnea and again we confirmed the correlation behavior. We made a statistical analysis of the exponent H and found that the differences between normals and sleep apnea patients were smaller than the differences between sleep stages. We conclude that sleep apnea does represent a shift of the heart rate regulation but not a general change of the regulation of the autonomous nervous system. It may be possible that we will be able to distin-

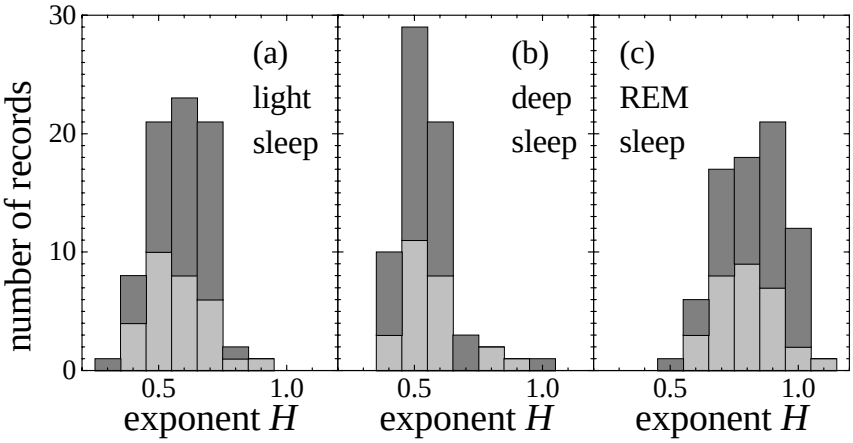

Fig. 8.9. Histograms of the fluctuation exponents H obtained from linear fits to log-log plots of $F(T)$ vs. T in the regime $70 < T < 300$ for (**a**) light sleep, (**b**) deep sleep, (**c**) REM sleep. The fitting range has been chosen to be above the regime of short-range correlations related to breathing and below the T values where the statistical errors become too large due to the finite length of the sleep stages. The data in (**a**) are based on all 30 records from healthy subjects (light gray) and on all 47 records from patients with moderate sleep apnea (dark gray). In (**b**) 10 records have been dropped since they where too short while in (**c**) only one record was too short and has been dropped

guish those patients which are likely to die from cardiovascular consequences of sleep apnea and those which do not die by using this advanced analysis to assess their heart rate regulation. This has to be investigated in long-term and outcome studies which have access to mortality data in these patients.

The results shown in Figs. 8.7 and 8.8 are representative for the 30 inter-beat records from 15 healthy individuals and 47 records from 26 individuals suffering from moderate sleep apnea with less than 22 apneas per hour that we analyzed [8.6]. The results are summarized in Fig. 8.9, where the histograms for the exponents H in the three sleep stages are shown. For light and deep sleep, the histograms are centered around $H \approx 0.5$ and show a large overlap. Both histograms are well separated from the histogram of REM sleep, that is centred around $H \approx 0.85$. We believe that our finding of the significant differences of the heartbeat correlations in the different sleep stages will lead to a better understanding of the different regulatory processes governing heart rate variability, which is an important diagnostic tool for pathophysiology. We also believe that the results will be useful to develop a sleep phase finder, that is based on the different heart rhythm in the different sleep stages, supplementing the quite tedious evaluation of the sleep stages by the standard electrophysiological procedures.

8.4 Timing Between Arrhythmic Events

8.4.1 Ventricular Tachycardia

Most of the fractal analysis of heart data has focused on analyzing the time between heartbeats. For example, it has been found that there are fractal scalings in the time between heartbeats and that these scalings are different between normal people and those with heart disease [8.29, 8.34]. There has been some previous fractal analysis on the times between events that disrupt the normal pattern of the heartbeat [8.35]. Here we describe how we used fractal methods to analyze the times between two different types of events that disrupt the heart rhythm.

The first type of events that we studied were episodes of rapid heart rate. These rapid heart rates are dangerous because they can lead to disorder in the heart contractions (ventricular fibrillation) so that the heart no longer pumps blood and death follows in a few minutes. A small computer, called a 'cardioverter defibrillator' can be implanted in the chest of patients at risk for these events. If the heart beats too fast this device produces an electrical shock to kick the heart back into a slower, safer rhythm. It can record the times when it was triggered and this can be played back with a radio transceiver when the patient returns to the hospital. We used this capability to determine the times between these events.

8.4.2 Premature Ventricular Contractions

The second type of events that we studied were episodes of additional heart beats. Both normal people and those with heart disease occasionally have additional heartbeats (premature ventricular contractions). Heartbeats can be detected by electrodes taped to the skin on the chest and recorded over a 24 hr period by a small monitor called a Holter recorder. We used a Rozzin Holter PC system to detect these additional heartbeats and determine the times between these events.

8.4.3 Probability Density Functions

As shown in Fig. 8.10, we found that the PDF of the time, t, between events of rapid heart rate is a straight line on a plot of $\log[\mathrm{PDF}(t)]$ vs. $\log(t)$, indicating that it has a fractal, power-law form over a scaling regime from 20 seconds to 10 days. At times greater than 10 days, the data seemed to shift from a power-law fractal form to one with a characteristic time scale. The fractal scaling regime means that over that large range of times there was no single average value for the time between these events. Most of the time it was a short time

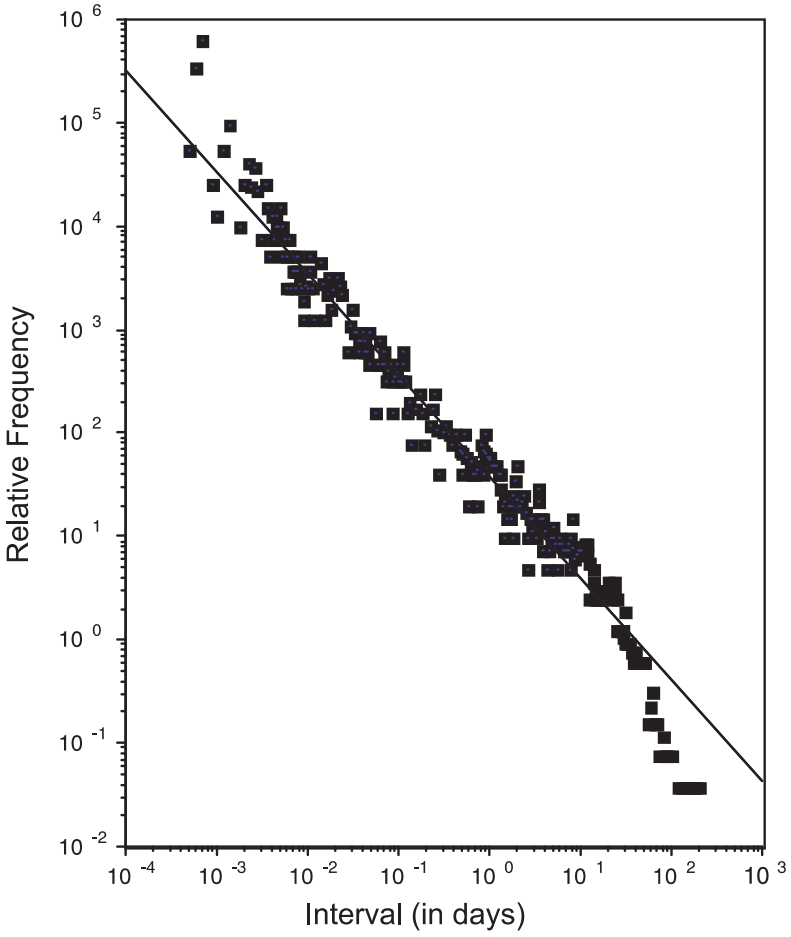

Fig. 8.10. The PDF (probability density function), the relative probability of the time, t, between episodes of rapid heart rate measured in 28 patients by implanted cardioverter defibrillators [8.7]. The straight line on this log-log plot over $20\,\mathrm{s} < t < 10\,\mathrm{days}$ indicates that the timing between these events has a fractal scaling over that time range. This means that no single, 'average' value can be used to characterize the time between these episodes. Such data can however, be meaningfully characterized by using the slope of the line on this plot, which is related to the fractal dimension

between these events. Less often it was longer. Very infrequently it was very long. This means that the rate of these events, that is, the number of events per day will be different if it is measured over one day, or one week, or one month, or one year. However, the meaningful way to characterize this data is by the slope of the plots of $\log[\mathrm{PDF}(t)]$ vs. $\log(t)$. This is related to the fractal dimension. We are presently studying how the fractal dimension depends on different disease conditions and medical therapies.

The short times between many of these events means that the local average rate of events is sometimes quite high. This observation had led to the conclu-

sion that there were 'storms' of these events [8.36]. However, the fractal scaling analysis shows that all the different times between these events are actually all part of the same PDF. This implies that the same physiological mechanisms produce both the short and long times between the events. It means that the high local average rate of events is therefore not due to a sudden physiological change [8.37]. The fractal form of this PDF raises important practical questions about how to evaluate the status of patients. A patient could be over-medicated in response to a high local average rate of events or under-medicated in response to a low local average rate of events. We are currently developing a measure, based on the slope and intercept of these PDF plots, to measure the relative risk of these events to the patient.

The PDF of the time, t, between the events of additional heartbeats was, to first order, also a straight line on a plot of $\log[\mathrm{PDF}(t)]$ vs. $\log(t)$. However, these plots had additional curvature and patient to patient variability that was not found in the PDF plots of the times between events of rapid heart rates [8.7].

8.4.4 Hurst Rescaled Range Analysis

We also used the Hurst rescaled range analysis to determine if there are fractal correlations in time between the episodes of rapid heart rate [8.7]. This analysis requires more data than determining the PDF. There were only enough events recorded from two patients with rapid heart rate to reliable perform this analysis. For both patients we found that $H = 0.6$, namely, that there were persistent correlations between the times between these events at all time scales. However, that result was statistically significantly different from the uncorrelated $H = 0.5$ at the $p = 0.05$ level for only one of those patients. It is a surprising result that the times between these events are so weakly correlated. It is as if the heart almost completely resets itself after each event so that the timing of the previous event has only a little effect on the timing of the next event.

We also used the Hurst rescaled range analysis to determine if there are fractal correlations in the time between additional heartbeats. We found that $0.7 < H < 0.8$ and that these persistent correlations were statistically significant ($p < 0.05$) [8.7]. This implies that the timing of the previous event has a strong effect on the timing of the next event.

8.5 Conclusion

Distributions of experimental data that have fractal rather than Gaussian distributions or that are long-range correlated cannot be meaningfully charac-

terized by their moments, such as the mean and variance. We have shown here how fractal measures, such as the power-law form of the PDF and the dispersion measured as a function of window size, by using the detrended fluctuations method (DFA) and the Hurst rescaled range method (R/S), are valid measures to characterize such fractal data.

In sleep physiology, these fractal measures have shown to be useful in the description of the heartbeat variability. While the PDF of the interbeat intervals has approximately Gaussian shape, long-range time autocorrelations in the records lead to fractal scaling of the dispersion function. Fourier transform has been employed to investigate the effect of obstructive sleep apnea on the heartbeat. Studying the heart rhythm in the different sleep stages (deep, light and REM sleep) that reflect different brain activities, we have shown that contrary to the common belief long-range correlations are present only in the 'dream'-REM stage, when the brain is very active as it is in the waking state. In contrast, in deep sleep the memory of the heart rates vanishes after a small number of beats that is below the order of the breathing cycle time. In light sleep finally, the heart rates seem to become uncorrelated as well, but the crossover occurs slightly above the breathing time. We believe that these findings will lead to a better understanding of the different regulatory processes governing heart rate variability and that they will be useful to develop a sleep phase finder.

In measuring heart arrhythmias, these fractal measures have shown that there is a fractal, power-law distribution in the times between episodes of rapid heart rate (ventricular tachycardia) and between episodes of additional heartbeats (premature ventricular contractions). It has also shown that the times between episodes of rapid heart rate are only weakly correlated, while the times between episodes of additional heartbeats are strongly correlated. Since this data is fractal it cannot be meaningfully characterized by its moments such as the mean and variance. That is, there is no single average rate per day of episodes of rapid heart rate or additional heartbeats. It is hoped that using fractal measures, such as the fractal dimension, to characterize this type of fractal data will lead to better diagnostic indicators and better ways to assess the effectiveness of medical therapies.

Acknowledgements. We would like to thank the National Institutes of Health (EY06234), the German Israeli Foundation, the Minerva Center for Mesoscopics, Fractals and Neural Networks, the Minerva Foundation, and the WE-Heraeus Foundation for financial support. The healthy volunteers were recorded as part of the SIESTA project funded by the European Union grant no. Biomed-2-BMH4-CT97-2040.

References

8.1 L.S. Liebovitch, *Fractals and Chaos Simplified for the Life Sciences* (Oxford University Press, New York, 1998).
8.2 L.S. Liebovitch and D. Scheurle, Complexity **5**, 34 (2000).
8.3 L.S. Liebovitch, A.T. Todorov, M.A. Wood, and K.A. Ellenbogen, in *Handbook of Research Design in Mathematics and Science Education*, edited by A.E. Kelly and R.A. Lesh, (Lawrence Erlbaum, Mahwah, 1999).
8.4 S. Havlin, R.B. Selinger, M. Schwartz, H.E. Stanley, and A. Bunde, Phys. Rev. Lett. **61**, 1438 (1998).
8.5 S.V. Buldyrev, A.L. Goldberger, S. Havlin, C.-K. Peng, and H.E. Stanley, in *Fractals and Science*, edited by A. Bunde and S. Havlin (Springer, Berlin, 1994).
8.6 A. Bunde, S. Havlin, J.W. Kantelhardt, T. Penzel, J.-H. Peter, and K. Voigt, Phys. Rev. Lett. **85**, 3736 (2000).
8.7 L.S. Liebovitch, A.T. Todorov, M. Zochowski, M. Scheurle, L. Colgin, M.A. Wood, K.A. Ellenbogen, J.M. Herre, and R.C. Bernstein, Phys. Rev. E **59**, 3312 (1999).
8.8 H.E. Hurst, R.P. Black, and Y.M. Simaika, *Long-term storage. An Experimental Study* (Constable, London, 1965).
8.9 J. Feder, *Fractals* (Plenum, New York, 1988).
8.10 C.-K. Peng, S.V. Buldyrev, S. Havlin, M. Simons, H.E. Stanley, and A.L. Goldberger, Phys. Rev. E **49**, 1685 (1994).
8.11 C.-K. Peng, S. Havlin, H.E. Stanley, and A.L. Goldberger, Chaos **5**, 82 (1995).
8.12 S.V. Buldyrev, A.L. Goldberger, S. Havlin, R.N. Mantegna, M.E. Matsa, C.-K. Peng, M. Simons, and H.E. Stanley, Phys. Rev. E **51**, 5084 (1995).
8.13 M.S. Taqqu, V. Teverovsky, and W. Willinger, Fractals **3**, 785 (1995).
8.14 F. Lombardi, A. Malliani, M. Pagani, and S. Cerutti, Cardiovasc. Res. **32**, 208 (1996).
8.15 R.L. Verrier, J.E. Muller, and J.A. Hobson, Cardiovasc. Res. **31**, 181 (1996).
8.16 American Academy of Sleep Medicine Task Force, Sleep **22**, 667 (1999).
8.17 A. Rechtschaffen and A. Kales, *A Manual of Standardized Terminology, Techniques, and Scoring System for Sleep Stages of Human Subjects*, (BIS/BRI, University of California, Los Angeles, 1968).
8.18 R.P. Vertes and K. Eastman, Behavior. Brain Sci. **23**, 867 (2000).
8.19 T. Young, M. Palta, J. Dempsey, J. Skatrud, S. Weber, and S. Badr, New Engl. J. Med. **328**, 1230 (1993).
8.20 V.K. Somers, M.E. Dyken, M.P. Clary, and F.M. Abboud, J. Clin. Invest. **96**, 1897 (1995).
8.21 C. Guilleminault, S.J. Connolly, R. Winkle, K. Melvin, and A. Tilkian, Lancet **I**, 126 (1984).
8.22 T. Penzel, G. Amend, K. Meinzer, J.H. Peter, and P. von Wichert, Sleep **13**, 175 (1990).
8.23 S. Akselrod, D. Gordon, F.A. Ubel, D.C. Shannon, A.C. Barger, and R.J. Cohen, Science **213**, 220 (1981),
8.24 Task Force of the European Society of Cardiology and the North American Society of Pacing and Electrophysiology, Circulation **93**, 1043 (1996).
8.25 M.H. Bonnet and D.L. Arand, Electroenceph. Clinical Neurophysiol. **102**, 390 (1997).
8.26 T. Penzel, J.H. Peter, and P. von Wichert, in *Colloque INSERM*, edited by C. Gaultier, P. Escourrou, and L. Curzi-Dascalova (John Libbey Eurotext, London, 1991), p. 79.
8.27 T. Penzel, A. Bunde, J. Heitmann, J.W. Kantelhardt, J.H. Peter, and K. Voigt, IEEE Comp. Cardiol. **26**, 249 (1999).
8.28 C.-K. Peng, J. Mietus, J.M. Hausdorff, S. Havlin, H.E. Stanley, and A.L. Goldberger, Phys. Rev. Lett. **70**, 1343 (1993).
8.29 S. Thurner, M.C. Feurstein, and M.C. Teich, Phys. Rev. Lett. **80**, 1544 (1998).
8.30 L.A. Amaral, A.L. Goldberger, P.Ch. Ivanov, and H.E. Stanley, Phys. Rev. Lett. **81**, 2388 (1998).
8.31 C.-K. Peng, J. Mietus, J.M. Hausdorff, S. Havlin, H.E. Stanley, and A.L. Goldberger, Physica A **249**, 491 (1998).
8.32 P.C. Ivanov, M.G. Rosenblum, L.A.N. Amaral, Z. Struzik, S. Havlin, A.L. Goldberger, and H.E. Stanley, Nature **399**, 461 (1999).

8.33 P.C. Ivanov, A. Bunde, L.A.N. Amaral, S. Havlin, J. Fritsch-Yelle, R.M. Baevsky, H.E. Stanley, and A.L. Goldberger, Europhys. Lett. **48**, 594 (1999).
8.34 A. Goldberger, C.-K, Peng, J. Hausdorff, J. Mietus, S. Havlin, and H.E. Stanley, in *Fractal Geometry in Biological Systems*, edited by P.M. Iannaccone and M. Khokha (CRC, Boca Raton, 1995).
8.35 K.M. Stein, L.A. Karagounis, J.L. Anderson, P. Kligfield, and B.B. Lerman, Circulation **91**, 722 (1995).
8.36 S.C. Credner, T. Klingenheben, O. Mauss, C. Sticherling, and S.H. Hohnloser, J. Am. Coll. Cardiol. **32**, 1909 (1998).
8.37 M.A. Wood, K.A. Ellenbogen, and L.S. Liebovitch, J. Am. Coll. Cardiol. **34**, 950 (1999).